Inorganic Chemistry
Cite This: Inorg. Chem. XXXX, XXX, XXX−XXX
Article
pubs.acs.org/IC

Combining the Single-Atom Engineering and Ligand-Exchange Strategies: Obtaining the Single-Heteroatom-Doped $Au_{16}Ag_1(S\text{-}Adm)_{13}$ Nanocluster with Atomically Precise Structure

Xi Kang,[⊥,†,‡] Lin Xiong,[⊥,§] Shuxin Wang,*[,†,‡] Yong Pei,*[,§] and Manzhou Zhu*[,†,‡]

[†]Department of Chemistry and Center for Atomic Engineering of Advanced Materials and [‡]Anhui Province Key Laboratory of Chemistry for Inorganic/Organic Hybrid Functionalized Materials, Anhui University, Hefei, Anhui 230601, China

[§]Department of Chemistry, Key Laboratory of Environmentally Friendly Chemistry and Applications of Ministry of Education, Xiangtan University, Xiangtan, Hunan 411105, China

Supporting Information

ABSTRACT: Obtaining cognate single-heteroatom doping is highly desirable but least feasible in the research of nanoclusters (NCs). In this work, we reported a new $Au_{16}Ag_1(S\text{-}Adm)_{13}$ NC, which is synthesized by the combination of single-atom engineering and ligand-exchange strategies. This new NC is so far the smallest crystallographically characterized Au-based NC protected by thiolate. The $Au_{16}Ag_1(S\text{-}Adm)_{13}$ exhibited a tristratified $Au_3{-}Au_2Ag_1{-}Au_1$ kernel capped by staple-like motifs including one dimer and two tetramers. In stark contrast to the size-growth from $Au_{18}(S{-}C_6H_{11})_{14}$ to $Au_{21}(S\text{-}Adm)_{15}$ via just the ligand-exchange method, combining single Ag doping on $Au_{18}(S{-}C_6H_{11})_{14}$ resulted in the size-decrease from $Au_{17}Ag_1(S{-}C_6H_{11})_{14}$ to $Au_{16}Ag_1(S\text{-}Adm)_{13}$. DFT calculations were performed to both homogold Au_{18} and single-heteroatom-doped $Au_{17}Ag_1$ to explain the opposite results under the same ligand-exchange reaction. Our work is expected to inspire the synthesis of new cognate single-atom-doped NCs by combining single-atom engineering and ligand-exchange strategies and also shed light on extensive understanding of the metal synergism effect in the NC range.

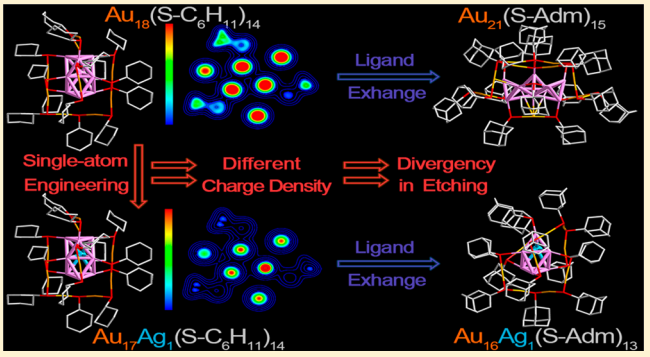

INTRODUCTION

Atomically precise nanoclusters (NCs) have attracted increasing attention from both fundamental and practical aspects owing to their unique properties and wide applications in biology, catalysis, and electronics.[1−8] During the past decades, a large number of thiolate-protected metal NCs have been synthesized, and many of them have been successfully crystallized.[9−17] In the wake of rapid development of monometallic NCs, bi- or multimetallic NCs have quickly emerged as new and prominent members due to their enhanced optical/catalytic properties.[1,5,18−25] Different strategies have been developed to synthesize new alloy NCs,[19−24,26,27] and among these alloying strategies, the "single-atom engineering" strategy has been attracting increasing attention.[18,19,23,24,26,27] For instance, a significant boost in fluorescence has been observed by doping a single Au atom into the center of $Ag_{25}(SR)_{18}$ and $Ag_{29}(SSR)_{12}(PPh_3)_4$.[23,24] In addition, the $Pd_1Au_{24}(SR)_{18}$ and $Pt_1Au_{24}(SR)_{18}$ show greatly enhanced catalytic activities compared with that of undoped $Au_{25}(SR)_{18}$.[18−20] Moreover, compared with proportionally doped alloy NCs (e.g., $Au_xAg_{25-x}(SR)_{18}$), NCs with only one heteroatom doping render a much simpler model for density functional theory (DFT) calculations, which have more potential for thoroughly understanding the structure−property relations.[19,23,24,26,27]

Recently, the metal-exchange method has become a versatile approach for synthesizing alloy NCs, which has been demonstrated with the ability to dope both high- and low-activity metals into parent NCs.[21−23,27] Nonetheless, in previous work, doping single heteroatom into homogold NCs is usually restricted to the different group metal (that is, doping Au (group 11) NCs with heteroatom from group 10 or 12).[19,20,27] To date, it has remained challenging to dope a single Ag/Cu atom into homogold NCs. This is probably due to the similar configuration of the outermost electrons in cognate elements (i.e., $d^{10}s^1$ of Cu, Ag, and Au), which is easy to pose a polydisperse formation in the metal-exchange products (e.g., $Ag_xAu_{25-x}(SR)_{18}$ or $Cu_xAu_{25-x}(SR)_{18}$).[27,28]

Previous works have demonstrated that doping cognate Ag/Cu into homogold NCs would significantly affect the electronic structure of the parent NCs.[1,5,27−29] Generally, the change of electronic structure will alter the binding ability of the metallic kernel with capped ligands.[30,31] For example, increased

Received: October 7, 2017

DOI: 10.1021/acs.inorgchem.7b02568
Inorg. Chem. XXXX, XXX, XXX−XXX

flexibility of the $Au_{38}(SR)_{24}$ NC was obtained by doping more silver atoms.[30] Moreover, when the central Au atom of Au_{25} was replaced by Pd, the resultant Pd_1Au_{24} exhibited remarkably enhanced activity in the ligand-exchange process, and this revealed that the heteroatom doping would have a profound effect on the ligand-exchange process.[31] Recently, the ligand-exchange method has frequently been used to synthesize new homo-Au NCs (e.g., Au_{18}–Au_{21}, Au_{25}–Au_{28}, Au_{38}–Au_{36}, and Au_{144}–Au_{133}).[14,32−34] However, it has rarely been tried on doped NCs, which impeded the full understanding of the metallic interaction effect as well as adequate analysis of the NC evolution. Inspired by the remarkable influence of single-atom engineering on the electronic structure of the homometal NCs, we rationalize that the products of the same ligand-exchange reaction on monometallic NCs and single-heteroatom-doped Au NCs could be different owing to the heteroatom effects. Furthermore, if the single Ag/Cu heteroatom-doped NC adopts another evolutional pattern compared with that of the homogold NC under the same ligand-exchange process, the mixture (the ligand-exchange resultants of homogold NC and doped NC) could be easily separated owing to the distinct size and surface structure. Thus, this strategy (combined the single-atom engineering and ligand-exchange methods) will not only facilitate the synthesis of a new class of cognate single-atom-doped NCs but also shed light on extensively understanding the metal synergism effect in the NC range.

Herein, different from etching $Au_{18}(S{-}C_6H_{11})_{14}$ with HS-Adm, which produces $Au_{21}(S\text{-}Adm)_{15}$, the same etching method on the single-heteroatom doped $Au_{17}Ag_1(S{-}C_6H_{11})_{14}$ (**$Au_{17}Ag_1$** for short) produces a different NC: $Au_{16}Ag_1(S\text{-}Adm)_{13}$ (**$Au_{16}Ag_1$** for short) with a decreased size. The preparative thin-layer chromatography (PTLC) was performed to separate the **$Au_{16}Ag_1$** from the ligand-exchange raw products (i.e., the mixture of $Au_{21}(S\text{-}Adm)_{15}$ and **$Au_{16}Ag_1$**), and the cognate single-atom engineering (in group 11) in Au-based NC was successfully achieved. The crystal structure of as-prepared **$Au_{16}Ag_1$** exhibits an unprecedented Au_6Ag_1 kernel protected by staple-like motifs including one dimer and two tetramers. To date, it is the smallest thiolated Au-based NC with identified X-ray crystal structure. Combining with DFT calculations, the HOMO–LUMO in **$Au_{16}Ag_1$** exhibits the sp ← d interband transition, same as the $Au_{18}(S{-}C_6H_{11})_{14}$. More importantly, the Vienna ab initio simulation package (VASP) was employed to perform the Bader charge analysis on $Au_{18}(S\text{-}CH_3)_{14}$ and $Au_{17}Ag_1(S\text{-}CH_3)_{14}$. The heterogeneous distribution of charge density around the Ag atom in **$Au_{17}Ag_1$** compared with the homogold one (i.e., $Au_{18}(S{-}C_6H_{11})_{14}$) is proposed as the fundamental reason for the difference in the ligand-exchange process. In addition, compared with the symmetrical $Au_{18}(S{-}C_6H_{11})_{14}$, no symmetry element was found in **$Au_{16}Ag_1$**, which illustrates that a significant portion of the **$Au_{16}Ag_1$** exhibited enantiomeric chirality.

EXPERIMENTAL SECTION

Chemicals. All reagents were purchased from Acros Organics or Sigma-Aldrich and used without further purification: tetrachloroauric (III) acid ($HAuCl_4{\cdot}3H_2O$, 99.99% metals basis), silver nitrate ($AgNO_3$, 99% metals basis), GSH (γ-Glu-Cys-Gly, M_w = 307.13 Da), cyclohexanethiol ($C_6H_{11}SH$, 95%), adamantane-1-thiol ($C_{10}H_{15}SH$, 95%), sodium cyanoborohydride ($NaBH_3CN$, 98%), methylene chloride (CH_2Cl_2, HPLC-grade, Aldrich), methanol (CH_3OH, HPLC, Aldrich), ethanol (CH_3CH_2OH, HPLC, Aldrich), hexane (C_6H_{14}, HPLC, Aldrich).

Synthesis of Ag(I)-SC_6H_{11} Complexes. For the Ag(I)SR complexes synthesis, AgCl (0.17 g, 1 mmol) was dissolved in 5 mL of CH_3OH, and cyclohexanethiol (135 μL, 1.1 mmol) was dissolved in 5 mL of CH_3OH and added dropwise to the solution under vigorous stirring (~1200 rpm). After reacting for 15 min, the solution mixture was washed several times with CH_3OH. Then, the final product was used directly.

Synthesis of the Single-Ag-Doped $Au_{17}Ag_1(S\text{-}C_6H_{11})_{14}$ NC. The $Au_{17}Ag_1(S{-}C_6H_{11})_{14}$ was synthesized by doping $Au_{18}(S{-}C_6H_{11})_{14}$ (prepared based on our previous report[35]) with Ag(I)SR. Specifically, $Au_{18}(S{-}C_6H_{11})_{14}$ (515 mg, 0.1 mmol) was dissolved in CH_2Cl_2 solution (5 mL), and Ag(I)SR (0.6 mg, 0.003 mmol) was added in under vigorous stirring at 273 K (ice-bath). After 5 min, the organic layer was separated and dried in a vacuum (note that the temperature was 273 K when dried) and then washed several times with CH_3OH.

Synthesis of the Single-Ag-Doped $Au_{16}Ag_1(S\text{-}Adm)_{13}$ NC. The as-obtained doping NCs were then used as the precursor to react with adamantanethiolate (HS-Adm). Typically, both 30 mg of the NC mixture and 0.5 g of HS-Adm were dissolved in 10 mL of CH_2Cl_2. The solution was heated to 40 °C and maintained at this temperature with vigorous stirring for 24 h. Then, the solvent was removed by rotary evaporation, and CH_3OH (20 mL) was added to the solution. Then, the mixture was centrifuged at 10000 rpm for 5 min; the supernatant was discarded, and the precipitate was washed with CH_3OH 3 times. A mixture of $Au_{16}Ag_1(S\text{-}Adm)_{13}$ and $Au_{21}(S\text{-}Adm)_{15}$ was obtained. The mixture of $Au_{16}Ag_1(S\text{-}Adm)_{13}$ and $Au_{21}(S\text{-}Adm)_{15}$ dissolved in 1 mL of CH_2Cl_2 was pipetted on the PTLC plate (10 cm × 20 cm), and the separation was conducted in the developing tank (developing solvent: CH_2Cl_2/CH_3OH = 10/1 v/v) for 60 min. A knife was used to cut the bands in the PTLC plate, and the products were extracted by pure CH_2Cl_2. Then, the collected solution was centrifugated at 10000 rpm to ensure that there were no nanoparticles in the solution. The organic layer was separated and dried in vacuum.

Crystallization of $Au_{16}Ag_1(S\text{-}Adm)_{13}$ NC. Single crystal of $Au_{16}Ag_1(S\text{-}Adm)_{13}$ NCs grown at room temperature for 2 days in CH_2Cl_2/CH_3CH_2OH. This step was repeated 3 times to obtain high-quality single crystals. Dark crystals were collected, and the structure of $Au_{16}Ag_1(S\text{-}Adm)_{13}$ was determined. The yield is 4.3% based on the Au element (calculated from $HAuCl_4$ to synthesize $Au_{18}(S{-}C_6H_{11})_{14}$ and the Au:Ag = 20:1 of the single-heteroatom doping process). The CCDC number of $Au_{16}Ag_1(S\text{-}Adm)_{13}$ NC is 1554060.

Theoretical Methods. All geometric optimizations of all NC structures were performed with the Perdew–Burke–Ernzerhof[36] functional, and the d-polarization included basis set (DND) was used for C, H, S elements. The DFT semicore pseudopotential (DSPP) approximation with some degree of relativistic corrections into the core was used for the Au and Ag elements implemented in the Dmol^3 package.[37,38] Time-dependent DFT calculations of the UV–vis optical spectrum and KS orbit implemented in the Amsterdam density functional (ADF) software packages with the PBE functional with the triple-ζ-polarized (TZP) basis sets. The TD-DFT calculations evaluated the lowest 1000 singlet-to-singlet excitation energies. The calculations on electron density maps were implemented by the Vienna ab initio simulation package (VASP) software.[39,40]

Characterization. All UV–vis absorption spectra of the NCs dissolved in CH_2Cl_2 were recorded using an Agilent 8453 diode array spectrometer, whose background correction was made using a CH_2Cl_2 blank.

Thermogravimetric analysis (TGA) was carried out on a thermogravimetric analyzer (DTG-60H, Shimadzu Instruments, Inc.) with 10 mg of **$Au_{16}Ag_1$** NC in a SiO_2 pan at a heating rate of 10 K min^{-1} from room temperature to 1073 K.

X-ray photoelectron spectroscopy (XPS) measurements were performed on a Thermo ESCALAB 250 configured with a monochromated Al Kα (1486.8 eV) 150 W X-ray source, 0.5 mm circular spot size, flood gun to counter charging effects, and analysis chamber base pressure lower than 1×10^{-9} mbar.

Inductively coupled plasma-atomic emission spectrometry (ICP-AES) measurements were performed on an Atomscan advantage

DOI: 10.1021/acs.inorgchem.7b02568
Inorg. Chem. XXXX, XXX, XXX–XXX

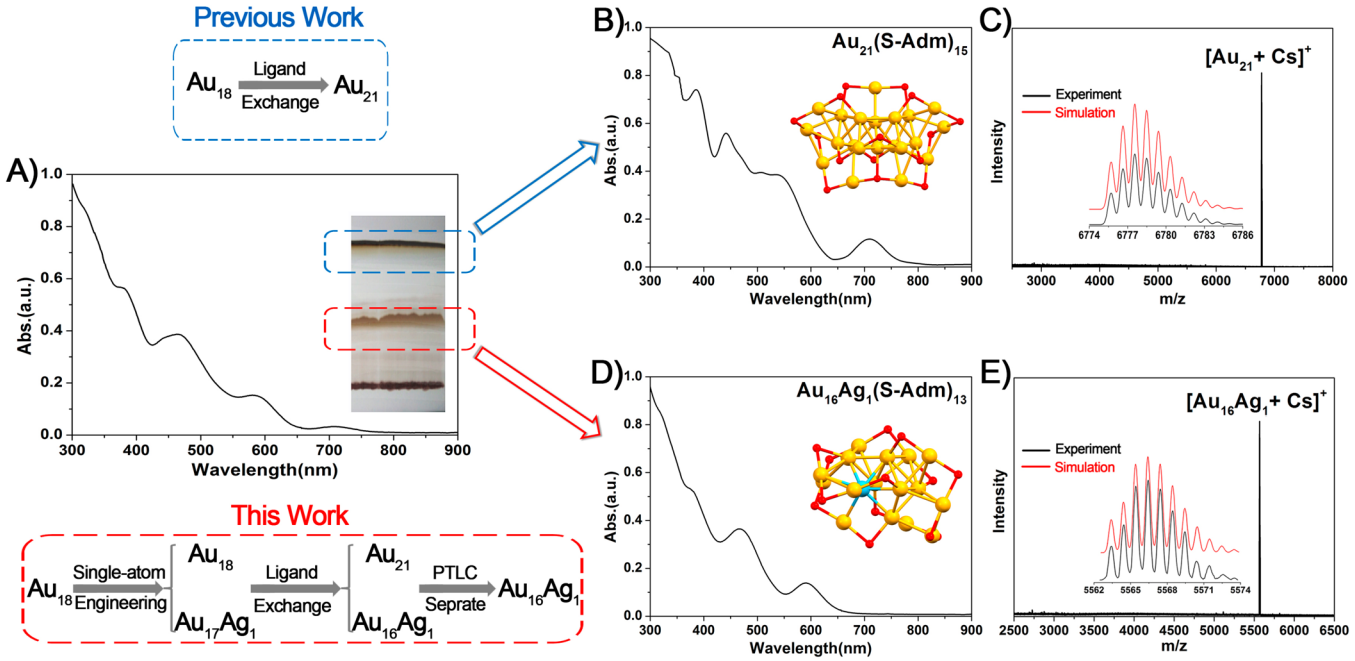

Figure 1. (A) UV−vis spectrum of the as-prepared mixture of $\mathbf{Au_{16}Ag_1}$ and $Au_{21}(S\text{-}Adm)_{15}$ NCs; inset: the PTLC separation result of this mixture. (B, C) UV−vis and ESI-MS spectra of separated $Au_{21}(S\text{-}Adm)_{15}$ NC; insets: (B) crystal structure and (C) experimental and simulated isotope patterns of $Au_{21}(S\text{-}Adm)_{15}$ NC. (D, E) UV−vis and ESI-MS spectra of separated $\mathbf{Au_{16}Ag_1}$ NC; insets: (D) crystal structure and (E) experimental and simulated isotope patterns of $\mathbf{Au_{16}Ag_1}$ NC. Color legend: orange sphere, Au; cerulean sphere, Ag; red sphere, S. For clarity, the carbon and hydrogen atoms are not shown.

instrument made by Thormo Jarrell Ash Corporation (USA). The $\mathbf{Au_{16}Ag_1}$ NC was digested by concentrated nitric acid, and the concentration of the $\mathbf{Au_{16}Ag_1}$ NC was set to ~0.5 mg L^{-1}.

Electrospray ionization time-of-flight mass spectrometry (ESI-TOF-MS) measurements were performed by MicrOTOF-QIII high-resolution mass spectrometer. The sample was directly infused into the chamber at 5 μL/min. For preparing the ESI sample, the NCs were dissolved in toluene (1 mg/mL) and diluted (v/v = 1:2) by dry methanol containing 5 mM CsOAc to ionize the NCs by forming the resultant Cs^+-NC.

The data collection for single-crystal X-ray diffraction was carried out on a Bruker Smart APEX II CCD diffractometer under liquid nitrogen flow at 130 K using graphite-monochromatized Cu Kα radiation (λ = 1.54178 Å). Data reductions and absorption corrections were performed using the SAINT and SADABS programs, respectively. The structure was solved by direct methods and refined with full-matrix least-squares on F^2 using the SHELXTL software package. All non-hydrogen atoms were refined anisotropically, and all the hydrogen atoms were set in geometrically calculated positions and refined isotropically using a riding model. The crystal structure of $\mathbf{Au_{16}Ag_1}$ was treated with PLATON SQUEEZE, and the diffuse electron densities from these residual solvent molecules were removed (with total void volume of 4913 $Å^3$ and squeezed electrons of 559 e).[41]

RESULTS AND DISCUSSION

Synthetic Strategy. Typically, the synthesis of $\mathbf{Au_{16}Ag_1}$ involves three steps (as shown in Figure 1). In the first step, controlled doping of $Au_{18}(S{-}C_6H_{11})_{14}$ with a small amount of $Ag^I(S{-}C_6H_{11})$ generates a mixture of $\mathbf{Au_{17}Ag_1}$ and unreacted $Au_{18}(S{-}C_6H_{11})_{14}$. It should be noted that (i) single-atom engineering has been achieved with the generation of $\mathbf{Au_{17}Ag_1}$, (ii) an excessive dose of $Ag^I(S{-}C_6H_{11})$ would produce $Au_{18-x}Ag_x(S{-}C_6H_{11})_{14}$ (x = 0−3) NCs instead of the $\mathbf{Au_{17}Ag_1}$ and unreacted $Au_{18}(S{-}C_6H_{11})_{14}$ NCs, and (iii) despite huge efforts, the separation of single-Ag-doped $\mathbf{Au_{17}Ag_1}$ from the mixture (i.e., $Au_{18-x}Ag_x(S{-}C_6H_{11})_{14}$) remains challenging. Accordingly, the following steps are necessary and significant to obtain the pure single-heteroatom-doped NC. In the second step, the ligand-exchange method (using HS-Adm ligand) was performed on this mixture, which converted the precursors into the mixed $\mathbf{Au_{16}Ag_1}$ and $Au_{21}(S\text{-}Adm)_{15}$ NCs. In the last step, we successfully separated the $\mathbf{Au_{16}Ag_1}$ from the mixture by the use of PTLC (shown in Figure 1).

As shown in Figure 1, $\mathbf{Au_{16}Ag_1}$ exhibits a different UV−vis spectrum from those of $Au_{18}(S{-}C_6H_{11})_{14}$ (shown in Figure S2) and $Au_{21}(S\text{-}Adm)_{15}$. The UV−vis of $\mathbf{Au_{16}Ag_1}$ shows two broad multiband optical absorptions centered around 465 and 590 nm and two shoulder bands at 320 and 380 nm. In addition, the TGA was performed to validate the purity of $\mathbf{Au_{16}Ag_1}$ NC. As shown in Figure S3, the weight loss (40.02%) is consistent with the theoretical value (40.63%), which confirms the purity of the product. Furthermore, the atomic ratio of Au/Ag (16:1) was verified by XPS and ICP measurements (Figures S4 and S5 and Table 1).

Table 1. Atomic Ratio of Au/Ag in the $\mathbf{Au_{16}Ag_1}$ NC Calculated by ICP and XPS Measurements

	Au atom	Ag atom
ICP experimental ratio	93.98%	6.02%
XPS experimental ratio	94.03%	5.97%
theoretical ratio	16/17 (94.12%)	1/17 (5.88%)

In the previous work, we used the HS-Adm ligand to convert $Au_{18}(S{-}C_6H_{11})_{14}$ into $Au_{21}(S\text{-}Adm)_{15}$.[32] Therefore, in this work it is safe to say that $\mathbf{Au_{16}Ag_1}$ was prepared from the $\mathbf{Au_{17}Ag_1}$ precursor (Figure 1). Interestingly, the ratio of $Au_{18}(S{-}C_6H_{11})_{14}$ and $\mathbf{Au_{17}Ag_1}$ in the mixed precursor (as well as the ratio of $Au_{21}(S\text{-}Adm)_{15}$ and $\mathbf{Au_{16}Ag_1}$ in the mixed

DOI: 10.1021/acs.inorgchem.7b02568
Inorg. Chem. XXXX, XXX, XXX−XXX

resultant) could be controlled by the initial single-heteroatom doping process. ESI-MS was performed to monitor the processes and identify the ratios. As shown in Figures S6 and S7, the intensities of the $\mathbf{Au_{17}Ag_1}$ and $Au_{18}(S{-}C_6H_{11})_{14}$ peaks in the ESI-MS spectrum positively correlates with the amount of the added $Ag^I(S{-}C_6H_{11})$. In addition, as the ligand-exchange resultant from these proportional precursors, the percentage of $\mathbf{Au_{16}Ag_1}$ in the mixed resultant is also dependent on the added $Ag^I(S{-}C_6H_{11})$.

Atomic Structure. The total structure of $\mathbf{Au_{16}Ag_1}$ was determined by the single-crystal X-ray diffraction (SC-XRD). As shown in Figure 2A, the kernel of $\mathbf{Au_{16}Ag_1}$ shows a

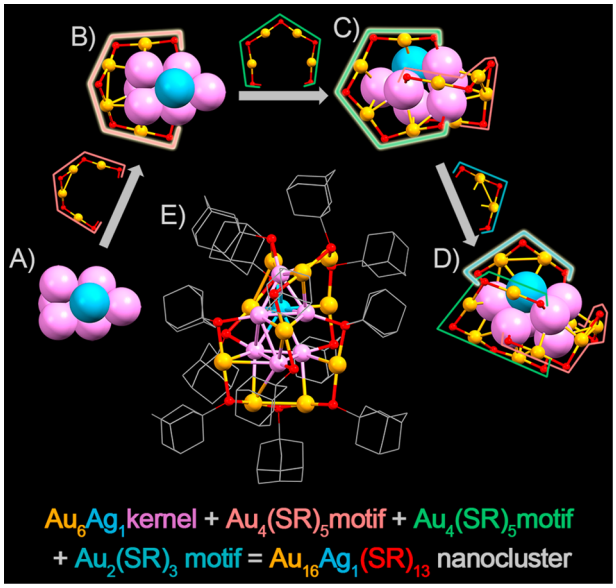

Figure 2. (A) Au_6Ag_1 kernel of $\mathbf{Au_{16}Ag_1}$ NC. (B–D) Au_6Ag_1 kernel with $Au_4(SR)_5$ staple motifs and $Au_2(SR)_3$ staple motif. (E) Total structure of the $\mathbf{Au_{16}Ag_1}$ NC. Color legend: orange sphere, Au on the shell; violet sphere, Au in the kernel; cerulean sphere, Ag; red sphere, S; pink and green highlighted lines, tetrameric $Au_4(S\text{-}Adm)_5$ staple motifs; blue highlighted line, bimeric $Au_2(S\text{-}Adm)_3$ staple motif.

tristratified arrangement, $Au_3{-}Au_2Ag_1{-}Au_1$, instead of the Au_3-M_3-Au_3 (M = Au/Ag) in $(AuAg)_{18}(S{-}C_6H_{11})_{14}$ NCs.[35,42,43] The interlayer distances of this tristratified structure are 2.64 and 2.36 Å, which are much more different compared with those of $Au_{18}(S{-}C_6H_{11})_{14}$ NC (2.49 and 2.52 Å, respectively). In particular, the interlayer distance of Au_1-M_3 (2.36 Å) is significantly shorter than the $Au_3{-}Au_3$ distance (2.52 Å) in $Au_{18}(S{-}C_6H_{11})_{14}$,[35,42] which is probably caused by the replacement of top Au_3 with only 1 Au. The Au_6Ag_1 kernel is further protected by two types of motifs: two tetrameric $Au_4(SR)_5$ staple motifs (Figure 2B and 2C) and one dimeric $Au_2(SR)_3$ staple motif (Figure 2D). The two $Au_4(SR)_5$ staples first constitute almost perpendicular planes and then fully wrap the Au_6Ag_1 kernel along with the other $Au_2(SR)_3$ staple. As a result of the irregular interaction between these three staple motifs, none of symmetry element was found in the structure of $\mathbf{Au_{16}Ag_1}$ NC (Figure 2E). Furthermore, no counterion was found in the unit cell of $\mathbf{Au_{16}Ag_1}$, which indicates the zero-valence state of $\mathbf{Au_{16}Ag_1}$ and is consistent with the ESI-MS and TGA results.

In the NC field, understanding the grand evolution from discrete atoms to atomically precise NCs is crucial. In the previous work, through monitoring the entire transformation from Au(I) complex precursors to small NCs, Xie and co-workers proposed a theory that the value of free valence electrons increases accompanied by the growth of the NC size (i.e., from 0 e^- to 2, 4, 6, and 8 e^-).[44] Unfortunately, the structural transformation remains uncertain at the atomic level because the accurate structures of these small-sized NCs are still not determined.[44] For the sake of fundamentally grasping the structure growth and variation (that is, understanding the essence of transformation from small molecular complexes to larger NCs), the atomically precise structures of the relatively smaller NCs are still highly desirable. The $\mathbf{Au_{16}Ag_1}$ in our work is so far the smallest crystallographically characterized Au-based NC protected by thiolate. Because of the zero-valence state, the free electron count of $\mathbf{Au_{16}Ag_1}$ is calculated as 4e (that is, 16 + 1 − 13 = 4), which renews the previous "isoelectronic" 4e small-sized NC family (i.e., $Au_{18}(S{-}C_6H_{11})_{14}$, $Au_{20}(TBBT)_{16}$, and $Au_{24}(SCH_2Ph\text{-}^tBu)_{20}$)[35,42,45,46] and validates the increment of free valence electrons from Au complexes to large-sized NCs.[44]

A previous report has already calculated the most probable structure of $\mathbf{Au_{17}Ag_1}$ in which the single Ag atom was arranged in the kernel and bonded with the $Au_2(SR)_3$ dimer.[47] Comparing the composition of the metallic kernel between $\mathbf{Au_{16}Ag_1}$ and $\mathbf{Au_{17}Ag_1}$, we found that the Au_8Ag_1 kernel transformed into the Au_6Ag_1 kernel (Figure 3A and C).

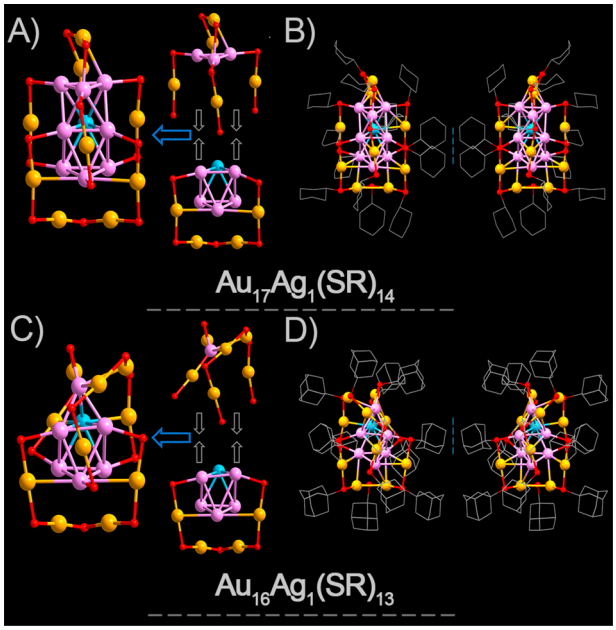

Figure 3. Structural comparison of $\mathbf{Au_{17}Ag_1}$ and $\mathbf{Au_{16}Ag_1}$ NCs. Comparing the top and bottom sections of (A) $\mathbf{Au_{17}Ag_1}$ and (C) $\mathbf{Au_{16}Ag_1}$ NCs; two enantiomers of (B) $\mathbf{Au_{17}Ag_1}$ and (D) $\mathbf{Au_{16}Ag_1}$ NCs. Color legend: orange sphere, Au on the shell; violet sphere, Au in the kernel; cerulean sphere, Ag; red sphere, S; gray sphere, C.

Remarkably, the position of the single Ag atom (or the configuration of the bottom two layers: $Au_3{-}Au_2Ag_1$) was retained. In other words, the tristratified $Au_3{-}Au_2Ag_1{-}Au_3$ kernel of $\mathbf{Au_{17}Ag_1}$ was etched into the $Au_3{-}Au_2Ag_1{-}Au_1$ configuration in $\mathbf{Au_{16}Ag_1}$ with the two bottom layers maintained. This configuration of M_7 core is observed for the first time, which is different with another Au_7 kernel in $Au_{20}(TBBT)_{16}$,[45] and both represent the smallest kernel in the thiolated NCs. Considering the alternation and reduction of the

DOI: 10.1021/acs.inorgchem.7b02568
Inorg. Chem. XXXX, XXX, XXX−XXX

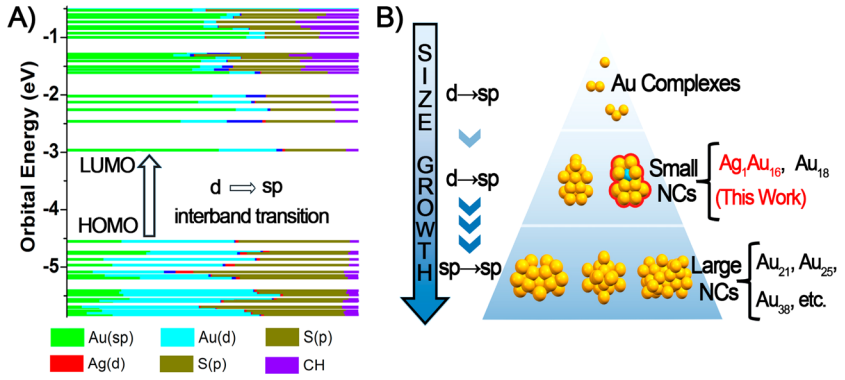

Figure 4. (A) Kohn–Sham electron states of $\mathbf{Au_{16}Ag_1}$ NC; (B) illustration of transition evolution from Au complexes to large Au NCs.

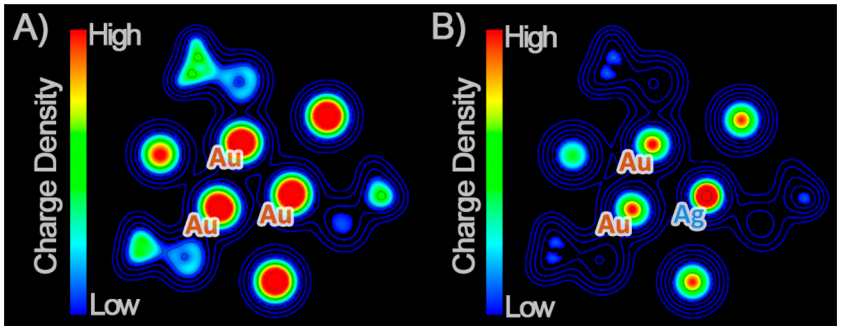

Figure 5. 2D charge density of metallic kernels of (A) $Au_{18}(S\text{-}CH_3)_{14}$ and (B) $Au_{17}Ag_1(S\text{-}CH_3)_{14}$ NCs.

kernel, we speculated that the metallic M_7 kernel might transform into M_3 layer-M_3 layer configuration (removing the top Au atom) or hexahedral M_5 configuration (removing two atoms from the bottom M_3 layer, like the M_9-M_7 process) followed by the further reduction of the NC size. In addition, the two enantiomers of $\mathbf{Au_{16}Ag_1}$ were compared with $\mathbf{Au_{17}Ag_1}$ (Figure 3B and D), and it can be observed that the configuration of $\mathbf{Au_{16}Ag_1}$ is more distorted than that of $\mathbf{Au_{17}Ag_1}$. Considering that the single-doped Ag heteroatom in $Au_{18}(S\text{–}C_6H_{11})_{14}$ would unlikely alter the NC configuration substantially,[43,47] the dramatic distortion probably occurred in the ligand-exchange process (i.e., from $\mathbf{Au_{17}Ag_1}$ to $\mathbf{Au_{16}Ag_1}$).

The Kohn–Sham electron states of $\mathbf{Au_{16}Ag_1}$ were probed via DFT computations. As shown in Figure 4A, the HOMO–LUMO energy gap was calculated as 1.54 eV. In addition, the HOMO–LUMO in $\mathbf{Au_{16}Ag_1}$ exhibits the sp ← d interband transition. Reviewing the previously reported NCs (Figure 4B and Table S2), the smaller Au NCs (with 2e or 4e free valence electrons) as well as the Au^I complexes typically exhibit the sp ← d interband transition.[35,42–45] By contrast, in larger NCs (free valence electrons equal to or greater than 6e), the HOMO–LUMO transition of the electronic excitation mode mainly involves sp ← sp intraband transition.[9,10,32–34] In our previous work, we have suggested that the emergence of sp ← sp intraband transition from sp ← d interband transition in the thiolate-stabilized NC is most likely caused by the increase of the NC free valence electron.[32] As to the $\mathbf{Au_{16}Ag_1}$ with 4e free valence electrons, the sp ← d interband transition verified our previous suggestion. Additionally, we further suggest that the HOMOs of small-sized Au-based NCs (smaller than $\mathbf{Au_{16}Ag_1}$) with 4e or 2e free valence electrons are more inclined to constitute by the d atomic orbitals.

Previous work has reported the growth result of $Au_{21}(S\text{-}Adm)_{15}$ from $Au_{18}(S\text{–}C_6H_{11})_{14}$.[32] Interestingly, the only product under the same ligand-exchange reaction on single-Ag-doped $\mathbf{Au_{17}Ag_1}$ is $\mathbf{Au_{16}Ag_1}$ with a decreased size. The only difference in the original reactant is the single heteroatom—doped Ag in the M_9 kernel. In this context, the charge densities of metallic M_9 kernels of $Au_{18}(S\text{–}C_6H_{11})_{14}$ and $\mathbf{Au_{17}Ag_1}$ were compared. As shown in Figure 5, we chose the corresponding kernel cross section of the two NCs to analyze their charge densities. It can be seen from the 2D charge density map of the two NCs that the charge distribution of the core is obviously different. The three kernel Au atoms in $Au_{18}(S\text{-}CH_3)_{14}$ have overlapping charge density, which indicates that the Au atoms in the core of $Au_{18}(S\text{-}CH_3)_{14}$ are averagely bonded by metal bonds. However, in the $Au_{17}Ag_1(S\text{-}CH_3)_{14}$ NC, the electron distribution around the doped Ag atom is obviously higher than that of the other two Au atoms, which shows strong polarization characteristics. The charge density distribution map of $Au_{17}Ag_1(S\text{-}CH_3)_{14}$ exhibits mainly ionic bonding between Au and Ag atoms due to the free electron motions, which is perhaps because of the difference of the charge density distribution around the Ag atom that results in the opposite direction of the ligand-exchange process. The 3D charge density maps are presented in Figure S8.

For analyzing whether there is charge transfer between Au and Ag atoms in the doping process from $Au_{18}(S\text{–}C_6H_{11})_{14}$ to $\mathbf{Au_{17}Ag_1}$, the charge density differences between $Au_{18}(S\text{-}CH_3)_{14}$ and $Au_{17}Ag(S\text{-}CH_3)_{14}$ were calculated, namely, $\Delta\rho = \rho(Au_{17}Ag\text{-}(S\text{-}CH_3)_{14})\text{-}\rho(Au_{18}(S\text{-}CH_3)_{14})$. As shown in Figure S9, after doping the single Ag, the charge at the doping site decreases significantly (the blue region indicates the decrease in charge of Au/Ag), and the charge of S (connecting to the doping site) increases (the yellow region indicates the increase in charge of S). Moreover, the charges at other positions were almost maintained. Consequently, the charge transfer between the Au and Ag atoms in the metallic kernel is small in the doping

DOI: 10.1021/acs.inorgchem.7b02568
Inorg. Chem. XXXX, XXX, XXX–XXX

process, whereas there is a significant charge transfer between the doping site and the S atoms because of the different electronegativities of Au and Ag atoms. On the basis of these results, no obvious charge transfer happens between Au and Ag atoms in the generation of alloyed $\mathbf{Au_{17}Ag_1}$. At the same time, Hirshfeld charge analysis (Figure S10) shows that the doping site charge increases from 0.037 to 0.083e and the S charge decreases from −0.029 to −0.073e, which is consistent with the differential charge density analyses. In addition, the atomic charges of the rest kernel atoms have no obvious change after the doping process.

CONCLUSIONS

In summary, $Au_{17}Ag_1(S{-}C_6H_{11})_{14}$ was first prepared by single-heteroatom doping strategy and further converted into $Au_{16}Ag_1(S\text{-}Adm)_{13}$ with ligand-exchange strategy. To date, the as-prepared $Au_{16}Ag_1(S\text{-}Adm)_{13}$ is the smallest crystallographically characterized Au-based nanocluster protected by thiolate. X-ray crystal structure of $Au_{16}Ag_1(S\text{-}Adm)_{13}$ reveals a tristratified $Au_3{-}Au_2Ag_1{-}Au_1$ kernel protected by staple-like motifs including one dimer and two tetramers. Contrary to the previous ligand-exchange on the $Au_{18}(S{-}C_6H_{11})_{14}$ ($Au_{21}(S\text{-}Adm)_{15}$ as the resultant), the product of the same ligand-exchange reaction on $Au_{17}Ag_1(S{-}C_6H_{11})_{14}$ is $Au_{16}Ag_1(S\text{-}Adm)_{13}$ with decreased size (instead of the size-increased species). The heterogeneous distribution of charge density around the Ag atom in the $Au_{17}Ag_1(S{-}C_6H_{11})_{14}$ nanocluster compared with the homogold $Au_{18}(S{-}C_6H_{11})_{14}$ is proposed as the fundamental reason for the difference in the ligand-exchange process. Morever, the $Au_{16}Ag_1(S\text{-}Adm)_{13}$ with HOMO−LUMO sp ← d interband transition exhibits "4e" free valence electrons, which renews the previous "isoelectronic" 4e small-sized nanocluster family. Furthermore, induced by the more distorted configuration (having no symmetry element) of $Au_{16}Ag_1(S\text{-}Adm)_{13}$, the enantiomeric chirality is dramatically enhanced relative to its precursors ($Au_{18}(S{-}C_6H_{11})_{14}$ or $Au_{17}Ag_1(S{-}C_6H_{11})_{14}$). Overall, the present study has filled the small-sized nanoclusters gap and, more significantly, provided a new strategy (combining the single-heteroatom engineering and ligand-exchange methods) to synthesize a new class of cognate single-atom-doped nanoclusters.

ASSOCIATED CONTENT

Supporting Information

The Supporting Information is available free of charge on the ACS Publications website at DOI: 10.1021/acs.inorgchem.7b02568.

Details of characterizations and DFT calculations (PDF)

Accession Codes

CCDC 1554060 contains the supplementary crystallographic data for this paper. These data can be obtained free of charge via www.ccdc.cam.ac.uk/data_request/cif, or by emailing data_request@ccdc.cam.ac.uk, or by contacting The Cambridge Crystallographic Data Centre, 12 Union Road, Cambridge CB2 1EZ, UK; fax: +44 1223 336033.

AUTHOR INFORMATION

Corresponding Authors

*E-mail: ixing@ahu.edu.cn.
*E-mail: ypnku78@gmail.com.
*E-mail: zmz@ahu.edu.cn.

ORCID

Shuxin Wang: 0000-0003-0403-3953
Yong Pei: 0000-0003-0585-2045
Manzhou Zhu: 0000-0002-3068-7160

Author Contributions

⊥X.K. and L.X. contributed equally to this work.

Notes

The authors declare no competing financial interest.

ACKNOWLEDGMENTS

M.Z. acknowledges financial support by NSFC (21372006, U1532141, and 21631001), the Ministry of Education, the Education Department of Anhui Province, 211 Project of Anhui University. Y.P. is supported by NSFC (21373176, 21422305), Hunan Provincial Natural Science Foundation of China (12JJ1003), and the Scientific Research Fund of Hunan Provincial Education Department (13A100).

REFERENCES

(1) Jin, R.; Zeng, C.; Zhou, M.; Chen, Y. Atomically Precise Colloidal Metal Nanoclusters and Nanoparticles: Fundamentals and Opportunities. *Chem. Rev.* **2016**, *116*, 10346−10413.

(2) Liu, P.; Qin, R.; Fu, G.; Zheng, N. Surface Coordination Chemistry of Metal Nanomaterials. *J. Am. Chem. Soc.* **2017**, *139*, 2122−2131.

(3) Fernando, A.; Weerawardene, K. L. D. M. N.; Karimova, V.; Aikens, C. M. Quantum Mechanical Studies of Large Metal, Metal Oxide, and Metal Chalcogenide Nanoparticles and Clusters. *Chem. Rev.* **2015**, *115*, 6112−6216.

(4) Zeng, C.; Chen, Y.; Kirschbaum, K.; Lambright, K. J.; Jin, R. Emergence of Hierarchical Structural Complexities in Nanoparticles and Their Assembly. *Science* **2016**, *354*, 1580−1584.

(5) (a) Yuan, X.; Dou, X.; Zheng, K.; Xie, J. Recent Advances in the Synthesis and Applications of Ultrasmall Bimetallic Nanoclusters. *Part. Part. Syst. Charact.* **2015**, *32*, 613−629. (b) Goswami, N.; Yao, Q.; Luo, Z.; Li, J.; Chen, T.; Xie, J. Luminescent Metal Nanoclusters with Aggregation-Induced Emission. *J. Phys. Chem. Lett.* **2016**, *7*, 962−975.

(6) Joshi, C. P.; Bootharaju, M. S.; Bakr, O. M. Tuning Properties in Silver Clusters. *J. Phys. Chem. Lett.* **2015**, *6*, 3023−3035.

(7) Chakraborty, I.; Pradeep, T. Atomically Precise Clusters of Noble Metals: Emerging Link between Atoms and Nanoparticles. *Chem. Rev.* **2017**, *117*, 8208−8271.

(8) Kurashige, W.; Niihori, Y.; Sharma, S.; Negishi, Y. Recent Progress in the Functionalization Methods of Thiolate-Protected Gold Clusters. *J. Phys. Chem. Lett.* **2014**, *5*, 4134−4142.

(9) (a) Heaven, M. W.; Dass, A.; White, P. S.; Holt, K. M.; Murray, R. W. Crystal Structure of the Gold Nanoparticle $[N(C_8H_{17})_4][Au_{25}(SCH_2CH_2Ph)_{18}]$. *J. Am. Chem. Soc.* **2008**, *130*, 3754−3755. (b) Zhu, M.; Aikens, C. M.; Hollander, F. J.; Schatz, G. C.; Jin, R. Correlating the Crystal Structure of A Thiol-Protected Au_{25} Cluster and Optical Properties. *J. Am. Chem. Soc.* **2008**, *130*, 5883−5885. (c) Tofanelli, M. A.; Ni, T. W.; Phillips, B. D.; Ackerson, C. J. Crystal Structure of the $PdAu_{24}(SR)_{18}^0$ Superatom. *Inorg. Chem.* **2016**, *55*, 999−1001.

(10) (a) Jin, R.; Liu, C.; Zhao, S.; Das, A.; Xing, H.; Gayathri, C.; Xing, Y.; Rosi, N.; Gil, R. R.; Jin, R. Tri-icosahedral Gold Nanocluster $[Au_{37}(PPh_3)_{10}(SC_2H_4Ph)_{10}X_2]^+$: Linear Assembly of Icosahedral Building Blocks. *ACS Nano* **2015**, *9*, 8530−8536. (b) Shichibu, Y.; Negishi, Y.; Watanabe, T.; Chaki, N. K.; Kawaguchi, H.; Tsukuda, T. Biicosahedral Gold Clusters $[Au_{25}(PPh_3)_{10}(SC_nH_{2n+1})_5Cl_2]^{2+}$ (n = 2−18): A Stepping Stone to Cluster-Assembled Materials. *J. Phys. Chem. C* **2007**, *111*, 7845−7847.

(11) (a) Joshi, C. P.; Bootharaju, M. S.; Alhilaly, M. J.; Bakr, O. M. $[Ag_{25}(SR)_{18}]^-$: the "Golden" Silver Nanoparticle. *J. Am. Chem. Soc.* **2015**, *137*, 11578−11581. (b) AbdulHalim, L. G.; Bootharaju, M. S.; Tang, Q.; Del Gobbo, S.; AbdulHalim, R. G.; Eddaoudi, M.; Jiang, D.-

DOI: 10.1021/acs.inorgchem.7b02568
Inorg. Chem. XXXX, XXX, XXX−XXX

e.; Bakr, O. M. $Ag_{29}(BDT)_{12}(TPP)_4$: A Tetravalent Nanocluster. *J. Am. Chem. Soc.* **2015**, *137*, 11970−11975.
(12) (a) Shichibu, Y.; Konishi, K. Electronic Properties of [Core +*exo*]-type Gold Clusters: Factors Affecting the Unique Optical Transitions. *Inorg. Chem.* **2013**, *52*, 6570−6575. (b) Yamazoe, S.; Matsuo, S.; Muramatsu, S.; Takano, S.; Nitta, K.; Tsukuda, T. Suppressing Isomerization of Phosphine-Protected Au_9 Cluster by Bond Stiffening Induced by a Single Pd Atom Substitution. *Inorg. Chem.* **2017**, *56*, 8319−8325.
(13) (a) Yang, H.; Wang, Y.; Chen, X.; Zhao, X.; Gu, L.; Huang, H.; Yan, J.; Xu, C.; Li, G.; Wu, J.; Edwards, A. J.; Dittrich, B.; Tang, Z.; Wang, D.; Lehtovaara, L.; Häkkinen, H.; Zheng, N. Plasmonic Twinned Silver Nanoparticles with Molecular Precision. *Nat. Commun.* **2016**, *7*, 12809. (b) Ren, L.; Yuan, P.; Su, H.; Malola, S.; Lin, S.; Tang, Z.; Teo, B. K.; Häkkinen, H.; Zheng, L.; Zheng, N. Bulky Surface Ligands Promote Surface Reactivities of $[Ag_{141}X_{12}(SAdm)_{40}]^{3+}$ (X = Cl, Br, I) Nanoclusters: Models for Multiple-Twinned Nanoparticles. *J. Am. Chem. Soc.* **2017**, *139*, 13288−13291.
(14) (a) Dass, A.; Theivendran, S.; Nimmala, P. R.; Kumara, C.; Jupally, V. R.; Fortunelli, A.; Sementa, L.; Barcaro, G.; Zuo, X.; Noll, B. C. $Au_{133}(SPh\text{-}tBu)_{52}$ Nanomolecules X-ray Crystallography, Optical, Electrochemical, and Theoretical Analysis. *J. Am. Chem. Soc.* **2015**, *137*, 4610−4613. (b) Zeng, C.; Chen, Y.; Kirschbaum, K.; Appavoo, K.; Sfeir, M. Y.; Jin, R. Structural Patterns at all Scales in a Nonmetallic Chiral $Au_{133}(SR)52$ Nanoparticle. *Sci. Adv.* **2015**, *1*, e1500045.
(15) (a) Desireddy, A.; Conn, B. E.; Guo, J.; Yoon, B.; Barnett, R. N.; Monahan, B. M.; Kirschbaum, K.; Griffith, W. P.; Whetten, R. L.; Landman, U.; Bigioni, T. P. Ultrastable Silver Nanoparticles. *Nature* **2013**, *501*, 399−402. (b) Conn, B. E.; Atnagulov, A.; Yoon, B.; Barnett, R. N.; Landman, U.; Bigioni, T. P. Confirmation of a de novo Structure Prediction for an Atomically Precise Monolayer-Coated Silver Nanoparticle. *Sci. Adv.* **2016**, *2*, e1601609.
(16) (a) Liao, L.; Zhuang, S.; Yao, C.; Yan, N.; Chen, J.; Wang, C.; Xia, N.; Liu, X.; Li, M.-B.; Li, L.; Bao, X.; Wu, Z. Structure of Chiral $Au_{44}(2,4\text{-}DMBT)_{26}$ Nanocluster with an 18-Electron Shell Closure. *J. Am. Chem. Soc.* **2016**, *138*, 10425−10428. (b) Liao, L.; Zhuang, S.; Wang, P.; Xu, Y.; Yan, N.; Dong, H.; Wang, C.; Zhao, Y.; Xia, N.; Li, J.; Deng, H.; Pei, Y.; Tian, S.-K.; Wu, Z. Quasi-Dual-Packed-Kerneled $Au_{49}(2,4\text{-}DMBT)_{27}$ Nanoclusters and the Influence of Kernel Packing on the Electrochemical Gap. *Angew. Chem., Int. Ed.* **2017**, *56*, 12644−12648.
(17) (a) Guan, Z.-J.; Zeng, J.-L.; Nan, Z.-A.; Wan, X.-K.; Lin, Y.-M.; Wang, Q.-M. Thiacalix[4]arene: New Protection for Metal Nanoclusters. *Sci. Adv.* **2016**, *2*, e1600323. (b) Wan, X.-K.; Cheng, X.-L.; Tang, Q.; Han, Y.-Z.; Hu, G.; Jiang, D.-e.; Wang, Q.-M. Atomically Precise Bimetallic $Au_{19}Cu_{30}$ Nanocluster with an Icosidodecahedral Cu_{30} Shell and an Alkynyl-Cu Interface. *J. Am. Chem. Soc.* **2017**, *139*, 9451−9454.
(18) Xie, S.; Tsunoyama, H.; Kurashige, W.; Negishi, Y.; Tsukuda, T. Enhancement in Aerobic Alcohol Oxidation Catalysis of Au_{25} Clusters by Single Pd Atom Doping. *ACS Catal.* **2012**, *2*, 1519−1523.
(19) Qian, H.; Jiang, D.-e.; Li, G.; Gayathri, C.; Das, A.; Gil, R. R.; Jin, R. Monoplatinum Doping of Gold Nanoclusters and Catalytic Application. *J. Am. Chem. Soc.* **2012**, *134*, 16159−16162.
(20) Kwak, K.; Choi, W.; Tang, Q.; Kim, M.; Lee, Y.; Jiang, D.-e.; Lee, D. A Molecule-Like $PtAu_{24}(SC_6H_{13})_{18}$ Nanocluster as an Electrocatalyst for Hydrogen Production. *Nat. Commun.* **2017**, *8*, 14723.
(21) Wang, S.; Meng, X.; Das, A.; Li, T.; Song, Y.; Cao, T.; Zhu, X.; Zhu, M.; Jin, R. A 200-Fold Quantum Yield Boost in the Photoluminescence of Silver-Doped Ag_xAu_{25-x} Nanoclusters: The 13th Silver Atom Matters. *Angew. Chem., Int. Ed.* **2014**, *53*, 2376−2380.
(22) (a) Kang, X.; Xiong, L.; Wang, S.; Yu, H.; Jin, S.; Song, Y.; Chen, T.; Zheng, L.; Pan, C.; Pei, Y.; Zhu, M. Shape-Controlled Synthesis of Trimetallic Nanoclusters: Structure Elucidation and Properties Investigation. *Chem. - Eur. J.* **2016**, *22*, 17145−17150. (b) Kang, X.; Silalai, C.; Lv, Y.; Sun, G.; Chen, S.; Yu, H.; Xu, F.; Zhu, M. $Au_{15}Ag_3(SPhMe_2)_{14}$ Nanoclusters-Crystal Structure and Insights into Ligand-Induced Variation. *Eur. J. Inorg. Chem.* **2017**, *2017*, 1414−1419.
(23) Bootharaju, M. S.; Joshi, C. P.; Parida, M. R.; Mohammed, O. F.; Bakr, O. M. Templated Atom-Precise Galvanic Synthesis and Structure Elucidation of a $[Ag_{24}Au(SR)_{18}]^-$ Nanocluster. *Angew. Chem., Int. Ed.* **2016**, *55*, 922−926.
(24) Soldan, G.; Aljuhani, M. A.; Bootharaju, M. S.; AbdulHalim, L. G.; Parida, M. R.; Emwas, A.-H.; Mohammed, O. F.; Bakr, O. M. Gold Doping of Silver Nanoclusters: A 26-Fold Enhancement in the Luminescence Quantum Yield. *Angew. Chem., Int. Ed.* **2016**, *55*, 5749−5753.
(25) Udayabhaskararao, T.; Sun, Y.; Goswami, N.; Pal, S. K.; Balasubramanian, K.; Pradeep, T. Ag_7Au_6: A 13-Atom Alloy Quantum Cluster. *Angew. Chem., Int. Ed.* **2012**, *51*, 2155−2159.
(26) Yan, J.; Su, H.; Yang, H.; Malola, S.; Lin, S.; Häkkinen, H.; Zheng, N. Total Structure and Electronic Structure Analysis of Doped Thiolated Silver $[MAg_{24}(SR)_{18}]^{2-}$ (M = Pd, Pt). *J. Am. Chem. Soc.* **2015**, *137*, 11880−11883.
(27) Wang, S.; Song, Y.; Jin, S.; Liu, X.; Zhang, J.; Pei, Y.; Meng, X.; Chen, M.; Li, P.; Zhu, M. Metal Exchange Method Using Au_{25} Nanoclusters as Templates for Alloy Nanoclusters with Atomic Precision. *J. Am. Chem. Soc.* **2015**, *137*, 4018−4021.
(28) Gottlieb, E.; Qian, H.; Jin, R. Atomic-Level Alloying and De-Alloying in Doped Gold Nanoparticles. *Chem. - Eur. J.* **2013**, *19*, 4238−4243.
(29) Kauffman, D. R.; Alfonso, D.; Matranga, C.; Qian, H.; Jin, R. A Quantum Alloy: The Ligand-Protected $Au_{25-x}Ag_x(SR)_{18}$ Cluster. *J. Phys. Chem. C* **2013**, *117*, 7914−7923.
(30) Zhang, B.; Bürgi, T. Doping Silver Increases the $Au_{38}(SR)_{24}$ Cluster Surface Flexibility. *J. Phys. Chem. C* **2016**, *120*, 4660−4666.
(31) Niihori, Y.; Kurashige, W.; Matsuzaki, M.; Negishi, Y. Remarkable Enhancement in Ligand-Exchange Reactivity of Thiolate-Protected Au_{25} Nanoclusters by Single Pd Atom Doping. *Nanoscale* **2013**, *5*, 508−512.
(32) Chen, S.; Xiong, L.; Wang, S.; Ma, Z.; Jin, S.; Sheng, H.; Pei, Y.; Zhu, M. Total Structure Determination of $Au_{21}(S\text{-}Adm)_{15}$ and Geometrical/Electronic Structure Evolution of Thiolated Gold Nanoclusters. *J. Am. Chem. Soc.* **2016**, *138*, 10754−10757.
(33) Zeng, C.; Li, T.; Das, A.; Rosi, N. L.; Jin, R. Chiral Structure of Thiolate-Protected 28-Gold-Atom Nanocluster Determined by X-ray Crystallography. *J. Am. Chem. Soc.* **2013**, *135*, 10011−10013.
(34) Zeng, C.; Qian, H.; Li, T.; Li, G.; Rosi, N. L.; Yoon, B.; Barnett, R. N.; Whetten, R. L.; Landman, U.; Jin, R. Total Structure and Electronic Properties of the Gold Nanocrystal $Au_{36}(SR)_{24}$. *Angew. Chem., Int. Ed.* **2012**, *51*, 13114−13118.
(35) Chen, S.; Wang, S.; Zhong, J.; Song, Y.; Zhang, J.; Sheng, H.; Pei, Y.; Zhu, M. The Structure and Optical Properties of the $[Au_{18}(SR)_{14}]$ Nanocluster. *Angew. Chem., Int. Ed.* **2015**, *54*, 3145−3149.
(36) Perdew, J. P.; Burke, K.; Ernzerhof, M. Generalized Gradient Approximation Made Simple. *Phys. Rev. Lett.* **1996**, *77*, 3865−3868.
(37) Delley, B. An All-Electron Numerical Method for Solving the Local Density Functional for Polyatomic Molecules. *J. Chem. Phys.* **1990**, *92*, 508−517.
(38) Delley, B. From Molecules to Solids with the $DMol^3$ Approach. *J. Chem. Phys.* **2000**, *113*, 7756−7764.
(39) Kresse, G.; Hafner, J. Ab Initio Molecular Dynamics for Open-Shell Transition Metals. *Phys. Rev. B: Condens. Matter Mater. Phys.* **1993**, *48*, 13115−13118.
(40) Kresse, G.; Furthmüller, J. Efficiency of Ab-Initio Total Energy Calculations for Metals and Semiconductors Using a Plane-Wave Basis Set. *Comput. Mater. Sci.* **1996**, *6*, 15−50.
(41) Sheldrick, D. M. Crystal structure refinement with SHELXL. *Acta Crystallogr., Sect. C: Struct. Chem.* **2015**, *71*, 3−8.
(42) Das, A.; Liu, C.; Byun, H. Y.; Nobusada, K.; Zhao, S.; Rosi, N.; Jin, R. Structure Determination of $[Au_{18}(SR)_{14}]$. *Angew. Chem., Int. Ed.* **2015**, *54*, 3140−3144.
(43) Xiang, J.; Li, P.; Song, Y.; Liu, X.; Chong, H.; Jin, S.; Pei, Y.; Yuan, X.; Zhu, M. X-ray Crystal Structure, and Optical and

DOI: 10.1021/acs.inorgchem.7b02568
Inorg. Chem. XXXX, XXX, XXX−XXX

Electrochemical Properties of the $Au_{15}Ag_3(SC_6H_{11})_{14}$ Nanocluster with a Core-Shell Structure. *Nanoscale* **2015**, *7*, 18278−18283.
(44) Luo, Z.; Yuan, X.; Yu, Y.; Zhang, Q.; Leong, D. T.; Lee, J. Y.; Xie, J. From Aggregation-Induced Emission of Au(I)-Thiolate Complexes to Ultrabright Au(0)@Au(I)-Thiolate Core-Shell Nanoclusters. *J. Am. Chem. Soc.* **2012**, *134*, 16662−16670.
(45) Zeng, C.; Liu, C.; Chen, Y.; Rosi, N. L.; Jin, R. Gold-Thiolate Ring as a Protecting Motif in the $Au_{20}(SR)_{16}$ Nanocluster and Implications. *J. Am. Chem. Soc.* **2014**, *136*, 11922−11925.
(46) Das, A.; Li, T.; Li, G.; Nobusada, K.; Zeng, C.; Rosi, N. L.; Jin, R. Crystal Structure and Electronic Properties of a Thiolate-Protected Au_{24} Nanocluster. *Nanoscale* **2014**, *6*, 6458−6462.
(47) Molina, B.; Tlahuice-Flores, A. Thiolated Au_{18} Cluster: Preferred Ag Sites for Doping, Structures, and Optical and Chiroptical Properties. *Phys. Chem. Chem. Phys.* **2016**, *18*, 1397−1403.

DOI: 10.1021/acs.inorgchem.7b02568
Inorg. Chem. XXXX, XXX, XXX−XXX